Article

Enhanced EIS analysis of microbial biofilms on an electrochemically in situ generated graphene interface

Jin Song, Yiwei Li, Fang Yin, Zhitao Zhang, Dingkun Ke, Dian-Bing Wang, Qipeng Yuan, and Xian-En Zhang

ACS Sens., **Just Accepted Manuscript** • DOI: 10.1021/acssensors.0c00570 • Publication Date (Web): 13 May 2020

Enhanced EIS analysis of microbial biofilms on an electrochemically *in situ* generated graphene interface

Jin Song[1,2], Yiwei Li[3], Fang Yin[2], Zhitao Zhang[2], Dingkun Ke[2], Dianbing Wang[2], Qipeng Yuan*[1], Xian-En Zhang*[2,4]

[1]Beijing Advanced Innovation Center for Soft Matter Science and Engineering, Beijing University of Chemical Technology, North Third Ring Road 15, Chaoyang District, Beijing 100029, China

[2]National Laboratory of Biomacromolecules, CAS Center for Excellence in Biomacromolecules, Institute of Biophysics, Chinese Academy of Sciences, 15 Datun Road, Chaoyang District, Beijing, 100101, China

[3]State Key Laboratory of Virology, Wuhan Institute of Virology, Chinese Academy of Sciences, Xiao Hong Shan No.44, Wuhan, 430071, China

[4]University of Chinese Academy of Sciences, No.19A Yuquan Road, Shijingshan District, Beijing, 100049, China

*Corresponding authors

KEYWORDS: Biofilm; Electrochemical impedance spectroscopy; Graphene; In situ synthesis; biosensor

ABSTRACT: Biofilms can cause many bacterial diseases, such as dental disease. An *in vitro* detection of biofilms may help to screen anti-biofilm drugs. An impedance measurement based on an Au electrode has been successfully used for *in vitro* real-time monitoring of animal and human cell growth. However, microbial growth on Au electrode produced poor signal because of the small size of microbial cells. We have recently demonstrated that graphene derivatives can be produced on a carbon electrode through a facile electrochemical activation, thus forming a reduced graphene oxide-carbon electrode (rGO-CE). Based on this fact, we hypothesized that an in vitro formed rugose graphene layer of rGO-CE may provide a large surface area for the growth of microbial biofilms and can therefore produce a strong impedance signal in response to a change in biomass. In this study, three oral bacteria, *Streptococcus mutans* (*S. mutans*), *Actinomyces viscosus* (*A. viscosus*) and *Lactobacillus fermentum* (*L. fermentum*), were cultured on the surfaces of rGO-CE. As a result, the impedance response signal of rGO-CE to the growth of *S. mutans* and *A. viscosus* was found to be 3.3 times and 6.0 times stronger than that of the Au electrode at 1.17 kHz and 54.7 kHz, respectively. In particular, the poorly adhering strain of *L. fermentum* also produced a detectable signal on the graphene electrode but not on the Au electrode at 1.17 kHz. Furthermore, destructions of the biofilms grew on the rGO-CE by cetylpyridinium chloride were successfully monitored by impedance changes. Overall, it is promising to develop a graphene-based impedance biosensor platform for biofilm study and anti-biofilm drug screening.

Microbial biofilms are an important survival strategy for microorganisms, and these biofilms consist of microorganisms and the accumulation of an extracellular matrix composed of one or more polymeric substances such as proteins, polysaccharides, humic substances, extracellular DNA and sometimes other molecules[1]. Contamination from a biofilm is a common occurrence, especially in clinics, where wound infections, bacterial endocarditis, cystic fibrosis airway infections, indwelling medical device infections, and mouth and genitourinary tract infection can be found[2]. The long-term accumulation of oral biofilm, a typical biofilm, will develop into dental plaque[3], which may lead to several detrimental effects on gingival tissues, teeth and their supporting structures. *The Global Burden of Disease Study in 2016* estimated that oral diseases affected at least 3.6 billion people worldwide. It is particularly important to efficiently and sensitively screen compounds that damage or destroy biofilms.

In recent decades, several approaches have been proposed to monitor and characterize biofilm growth. These methods include weighing dried cells, manual or automated cell counting and several optical techniques such as turbidity and fluorescence measurements[4]. In addition to these approaches, techniques exist that correlate parameters such as the oxygen consumption rate or the carbon dioxide production rate to the cell density[5, 6]. Even so, the above methods are tedious, time-consuming, manual operations and labour-intensive. Electrochemical impedance spectroscopy (EIS) has been used to assess cell growth due to it being a fast, sensitive and label-free technique that can characterize (bio)physical processes at the substrate-biomaterial interface. Briefly, when the cells are exposed to an electric field generated by a continuous sweeping of an alternating current voltage over a range of frequencies, the cells act as insulating particles that impede the flow of electric current

when they distribute on the electrode, thus increasing the impedance of the system. In recent years, EIS had been used to study the biofilms formed on various metal electrode surfaces, such as stainless steel [7-9], Indium-tin-oxide (ITO) [10,11], platinum and Au [12]. Au electrode has been successfully used in electrochemical impedance spectroscopy (EIS) assays of growth of animal cells, yet being problematic in the assays of bacterial biofilms due to much smaller size and less interfacial adhesion of bacterial cells than that of animal cells. Even if bacteria can form a biofilm, the impedance signal of the biofilm on the Au electrode is insufficient in impedance assays[13-17]. This would also cause response delay and deteriorate the sensitivity in biofilm monitoring, especially in the early stage detections of the biofilm. On the other hand, unideal microstructure and/or microenvironment of the interface of the electrodes may also be a reason [18]. Therefore, it is necessary to improve the sensing interface *per se* or develop novel ones to enhance the sensitivity of biofilm detections. Graphene has long been attracting attentions from electrochemical analysts due to its outstandingly high conductivity and biocompatibility[19-21]. Wang et al [22] developed an interface of graphene-based electrical impedance sensor for metastatic cancer diagnosis at single-cell resolution, the collected electrical signals from graphene bio-interface were about two times stronger than those from the Au interface. As far as we have known, there are few studies using graphene interfaces to detect biofilms. Therefore, we attempted to construct graphene-modified electrode interface to enhance the electrochemical sensing effect of bacterial biofilms. Initially, suspensions were prepared by coating chemically synthesized graphene oxide (GO) on pretreated Au or glassy carbon electrodes; unfortunately, heterogeneous modifications of GO have been found to be insufficiently robust on classic electrode interfaces, which has hindered their application (Figure S1). Based on this fact, an *in situ* electrochemical method is adopted in our study to prepare a graphene-modified electrode. The proposed method was verified herein featuring simplicity in fabrication and low cost while satisfying the EIS assay of bacterial biofilms.

Here, we fabricated a graphene-modified carbon rod with a wrinkled and rough electrode surface based on our previous finding that the surface of a carbon electrode (CE) will form a graphene derivative layer after simple electrochemical activation[23]. Compared with a graphene layer formed by a drop-casting modification from chemically synthesized GO, the *in situ* modified graphene layer avoids exfoliation and fissuring. *Streptococcus mutans (S. mutans), Actinomyces viscosus (A. viscosus)* and *Lactobacillus fermentum (L. fermentum)*, the oral pathogens and the model of bacterial biofilm formation [24-26], were studied in this work. We assume the rGO-CE should have better electrochemical activity compared to Au electrodes and a bare CE, and its wrinkled surface can accommodate more biomass so that more bacteria can be captured to facilitate the formation of a biofilm; thus, the detection sensitivity can be improved. Results proved the predictive advantages of this method, when it was used to EIS detection of biofilms of oral bacteria. Compared to the Au electrode and bare CE, rGO-CE showed a significantly higher impedance signal to the biofilm of the three bacteria at a characteristic frequency. Furthermore, parallelly evidence by crystal violet staining showed the growth tendencies of the bacteria follow the results revealed via the EIS measurements. This work is particularly important for detecting biofilms with poor adhesion, especially for the low impedance signals generated by Au electrodes used in conventional impedance testing[15, 27]. In addition, we use cetylpyridinium chloride for biofilm damage experiments. The results show that the relative impedance change rate of rGO-CE is also better than that of the Au electrode and CE.

EXPERIMENTAL

All materials, reagents, instruments and experimental methods used in this study are described in detail in the Supporting Information.

RESULTS AND DISCUSSION

Characterization of the electrode. The morphologies of the working electrodes were investigated by SEM (Figures 1a-d). The surface of the CE before treatment was uneven as shown in Figure 1b, and even the Au electrode, which looked extremely smooth, had a surface that was defective under SEM magnification (Figure 1a). After oxidation, the surface roughness of the CE was increased, and there were significant wrinkles (Figure 1c). It has been reported that dramatic changes in electrode surface roughness and uniformity are caused by electrochemical etching effects at extreme potentials[28-30]. Subsequently, we electrochemically reduced the electrode and obtained a coarser and fluffy layered structure as shown in Figure 1d, which indicated that the surface of the anodized CE was forced to be rearranged by electrochemical reduction. The same phenomenon has been reported for chemically reduced graphene oxide (crGO) samples[31]. Moreover, the structure was similar to chemically synthesized reduced graphene[32-34]. This was also consistent with the SEM results of our previous electroactive carbon paste electrodes[23]. Through an *XPS* analysis (Figure S2), we obtained detailed information on the elements and structural composition of the structure obtained by an electrochemical treatment. The largest changes in the peak intensity were the C 1s and O 1s bands (Figure S2a). Figure S2b shows that the oxygen content of GO-CE after oxidation was significantly higher than that of CE and rGO-CE due to the increase in C-O-H/C-O-C (286.5 eV) and C=O (288.0 eV) functional groups (Figures S2c, d). This was because prolonged anodization would cause lattice rupture and the formation of edge plane defects, which would become hydroxyl and carboxyl groups [35, 36]. The oxygen content of reduced rGO-CE was lower than that of GO-CE, indicating that the removal of edge defect sites was not complete (Figure S2e). Moreover, because of the low degree of redox reaction, changes in the carboxyl functional group throughout the electrochemical process were not detected[23]. The increase in peak intensity of C-C (285.0 eV) and the decrease in peak intensity of C=C (284.7 eV), and subsequent decrease and their increase, respectively, revealed the interconversion of sp^3 carbon and

sp^2 carbon during redox. Thus, an *in situ XPS* analysis further verified the graphene nature of the surface structure on the CEs obtained by redox processing.

We also studied the electrochemical behaviour of several working electrodes in a chemically inert electrolyte containing a 5 mM $[Fe(CN)_6]^{4/3-}$ probe, for the further elucidate the difference in the activated surface of the CE after a redox reduction. As shown in Figure S3a, the response curent of the CE was very weak. However, after an oxidation treatment, the current dramatically increased. Both GO-CE and rGO-CE exhibited greatly improved electrical conductivity, but GO itself was insulated [16]. This could be attributed to the electrochemical etching effect due to the dissociation of graphite particles on the electrode surface, which resulted in more defects/edge plane exposure and led to an increase in the specific surface area of the electrode. Then,

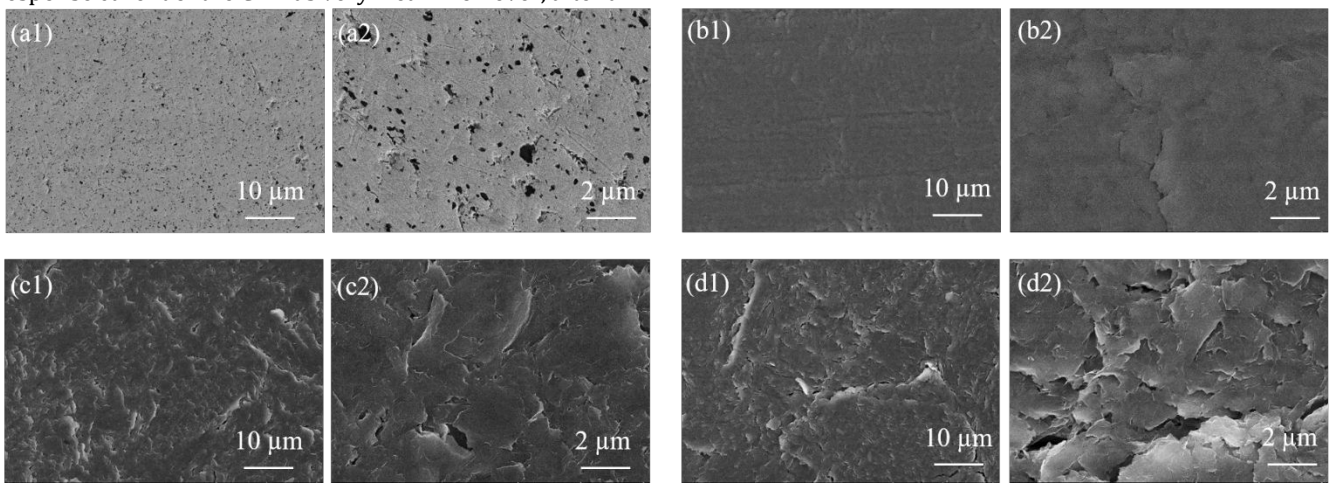

Figure 1. SEM images of (a1, a2) Au electrode, (b1, b2) CE, (c1, c2) GO-CE and (d1, d2) rGO-CE. The images of a2, b2, c2 and d2 are at a higher magnification.

the $[Fe(CN)_6]^{4/3-}$ probe was used to reveal the electrochemical performance of the three working electrodes. As seen in Figure S3b, the CE showed weak and irreversible (the peak potential difference was ΔE≈130 mV) oxidation and reduction reactions. After the oxidation treatment, a pair of excellent redox peaks appeared, indicating an increase in the sensitivity and reversibility of GO-CE (ΔE<100 mV). This was due to the etching effect, which increased the surface area of the electrode during the oxidation process. Furthermore, through a subsequent reduction treatment, rGO-CE obtained a further increase in peak intensity. This indicated that the *in situ* generated rGO further reduced the electrode surface resistance because it had better conductivity than GO. In summary, the *in situ* produced graphene-modified interface was verified to be successfully obtained.

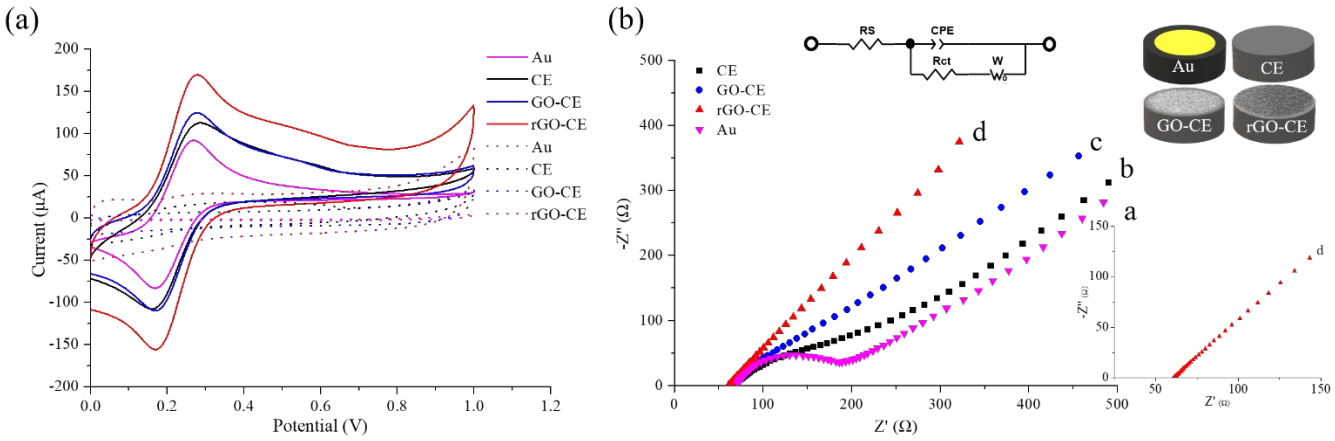

Figure 2. a, CV curves (3th) of the pristine CE, GO-CE and rGO-CE. Dashed lines are the responses in a 0.1 M KCl solution, and solid lines represent the responses in a 0.1 M KCl containing 20 mM potassium ferrocyanide. The curves are all recorded at a scan rate of 20 mV/s. b, Typical Nyquist plots of the bare Au (a), CE (b), GO-CE (c) and rGO-CE (d) in a 50 mM phosphate buffer (pH 7.0) containing 5 mM $[Fe(CN)_6]^{4-/3-}$ and 0.1 M KCl within a frequency range of 100 kHz to 0.1 Hz.

To further illuminate the difference between the CE surfaces, the electrochemically active surface area (EASA) of the different working electrodes was calculated. CV curves were recorded in a 0.1 M KCl solution containing 20 mM potassium ferrocyanide at ambient temperature (scan rate is 20 mV/s). The value of the electroactive surface area was calculated according to the *Randles-Sevcik* equation[37]:

$$Ip=2.69\times10^5 AD^{\frac{1}{2}}n^{\frac{3}{2}}\upsilon^{\frac{1}{2}}C \quad (1)$$

where A is the area of the electrode (cm^2), D is the diffusion coefficient of the molecule in solution (0.65×10^5 cm^2/s) [38], n is the number of electrons participating in the redox reaction, υ is the scan rate (V/s), and C is the concentration of the probe molecule in the bulk solution (mol/cm^3). According to the results given in Figure 2a, the EASAs of the bare Au electrode, CE, GO-CE and rGO-CE were 0.048 cm^2, 0.049 cm^2, 0.060 cm^2 and 0.068 cm^2 respectively. Compared to the bare Au electrode and CE, the GO-CE showed an ~25 and ~22% increase in EASA, respectively, and the following rGO-CE showed an ~42 and ~39% increase, respectively. Undoubtedly, both electrochemical activation processes contributed to the increase in EASA of the electrode, and in the electro-oxidation process, an etching effect could be very beneficial. This effect was very helpful for obtaining an enlarged electrode surface area.

EIS assays were carried out in parallel. The Nyquist plots of the bare Au electrode, CE, GO-CE and rGO-CE presented in Figure 2b demonstrated that the CE showed a flat and slightly larger semi-circular area recorded in the high frequency zone relative to that of the bare Au electrode, which represented a large electron transfer resistance (R_{ct}) and was due to the relatively weak conductivity of pristine graphite [28] and its uneven surface. However, on GO-CE, the R_{ct} decreased because pure GO is a material with often less conductivity than its parental graphite [23, 39]. Therefore, the obviously reduced R_{ct} could be attributed to the electro-etching effect caused by the anodizing treatment, which produced an increase in the specific surface area of the electrode. rGO-CE exhibited an almost straight line, which was characteristic of a diffusion limiting step in the electrochemical process[40].

Based on all the characteristics of the formed rGO-CE, we assumed that the rough surface formed by this wrinkled microtopography was very likely to provide a larger interface for the growth of microbial biofilms, increase the loaded biomass and thus significantly improve the detection of biofilms. Therefore, we tried to use rGO-CE to culture three models of oral bacterial biofilms to verify our hypothesis.

Biofilm formation and morphology analysis. To obtain a robust biofilm for subsequent experiments, we selected 12 h, 12 h and 20 h as the biofilm culture periods for *S. mutans, L. fermentum* and *A. viscosus*, respectively (Figures S4a-c). In addition, we also used crystal violet staining to verify the biofilm formation time of the three oral bacteria. The results showed that biofilm was present in the corresponding inoculation wells, which appeared to be weaker in the BHI medium without an additional supply of carbon (Figures S4d, e). However, *L. fermentum* did not appear to show any signs of biofilm formation, even in the wells with high concentrations of sucrose (Figure S4f). The increase in the cell index (CI) value of *L. fermentum* was most likely due to its dense proliferation behaviour on the microelectrode surfaces.

CLSM was chosen to characterize the actual biofilm morphology *in situ* due to its non-invasive and non-destructive characteristics, and it is actually considered an effective tool for the *in situ* study of biofilms. We cultured the three bacteria for 12 h, 20 h and 12 h to observe the actual morphology of the three biofilms. Syto9 plus propidium iodide (PI) offers the possibility of selectively staining live and dead bacteria and has therefore been widely used to analyses bacterial viability. Syto9 plus PI which kept bacterial cells with intact cytoplasmic membranes (emitting green fluorescence) to be differentiated from bacteria with damaged membranes (emitting red fluorescence) [41]. Syto9 is a DNA-intercalating dye that penetrates all bacterial membranes and stains the cells green, while PI only penetrates cells with damaged membranes and displaces Syto9 because of its stronger affinity to DNA and thus quenches S-yto9 emission, producing red fluorescing cells. As shown in Figure 3a, *S. mutans* was more likely to form macro-colonies in the presence of sucrose, while the other two bacteria formed a uniform dense biofilm (Figures 3b, c; Figure S4d). After 12 h, 20 h and 12 h of culture, the biofilm was not stained red by PI, and the colour of the merge was also green, so it can be stated that a stable biofilm was formed, which was also consistent with the biofilm formation time obtained from Figure S4.

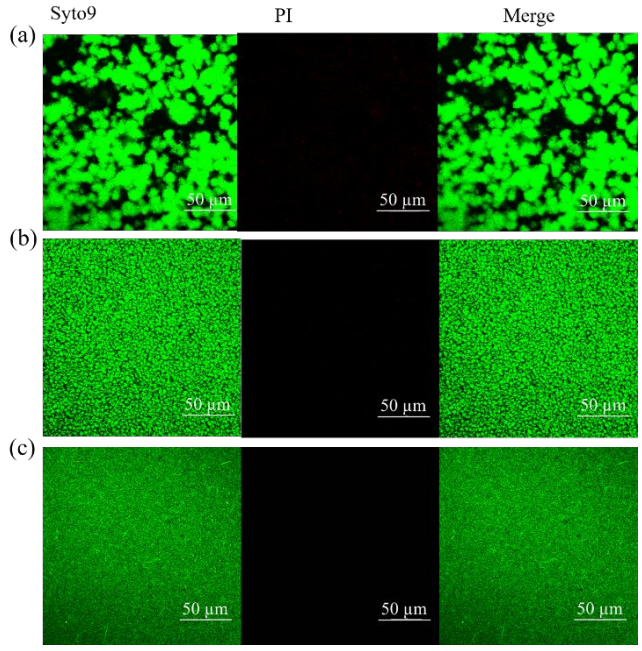

Figure 3. Morphology of oral bacterial biofilms measured with inverted confocal laser scanning microscopy (CLSM).

Projections of biofilms structures stained with a BacLight bacterial Viability Kit. Fluorescent dyes were cocultured with *S. mutans* (a), *A. viscosus* (b) and *L. fermentum* (c) for 12 h, 20 h and 12 h, respectively, and the distribution of green (SYTO 9 for live bacteria), red and yellow/colocalized (PI for dead bacteria) was observed in the biofilm.

Biomass analysis of biofilm on an electrode surface. The assay for biofilm formation used for this study was adapted from an O'Toole and Kolter method [42], which was based on the ability of bacteria to form biofilms on solid surfaces, which were then stained with crystal violet (Cvio). Cvio binding to negatively charged molecules, including nucleic acids and acidic polysaccharides, it thereby serves as an overall measure of the whole biofilm. As shown in Figure S5, the biomass of the three bacteria attached to rGO-CE was larger than that of Au and CE. Specifically, the biomass of biofilms attached to rGO-CE of *S. mutans* and *A. viscosus* was 1.1 times and 1.2 times higher than that of Au electrodes, respectively, and 1.2 times and 1.8 times higher than that of CE, respectively, while the biofilm biomass of *L. fermentum* was 1.7 times that of Au electrodes and 2.0 times that of CE.

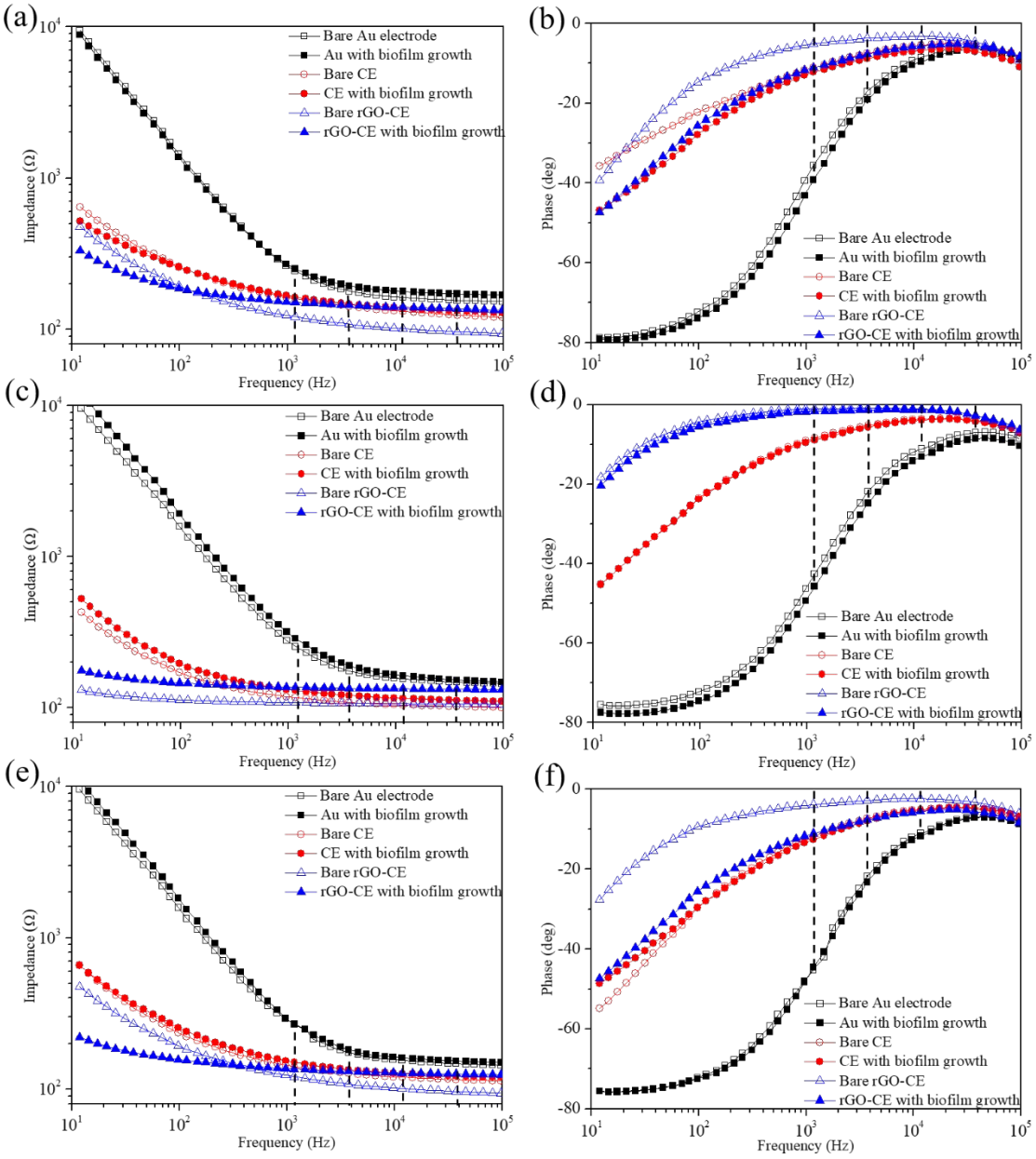

Figure 4. Mean (n=5) impedance amplitude and phase spectrum of the three kinds of bacteria. Bode impedance spectra of *S. mutans* (a), *A. viscosus* (c) and *L. fermentum* (e) on the Au, CE and rGO-CE interface. Phase spectra of *S. mutans* (b), *A. viscosus* (d) *and L. fermentum* (f) on the Au, CE and rGO-CE interface.

This was mainly due to the relatively large and rough surface of rGO-CE facilitating the adhesion of bacteria, since the roughness helped provide niches where bacteria could adhere to and get protected from the outside world. This also confirmed our hypothesis that rGO-CE increased the biomass when compared to that of the Au electrode.

EIS detection of biofilm. The detection of bacteria by an impedance assay is based on the phenomenon that live cells become polarized in an electric field, whereas dead cells do not respond to the electric field as sensitively as viable cells because they lack an intact cell membrane [43, 44]. Polarization occurs at a certain frequency which is characteristic for the type of bacteria. When the characteristic frequency is exceeded, the charges at the cell membrane cannot follow the electric field, and the bacteria stop contributing to the measured impedance. Therefore, it is especially important to make a full frequency impedance spectrum and select the appropriate characteristic frequency.

After 12 h or 20 h bacterial culture, an increase in impedance magnitude was achieved, indicating the bacteria were attached and biofilms were formed. A clear distinction between the impedance amplitude and phase value of the biofilm produced by the three bacteria was observed in a frequency ranging of 1~100 kHz (Figure 4) when compared to the bacteria-free state. A greater impedance amplitude was observed from rGO-CE, compared with that of Au and CE; however, the change rule of the phase value was inconsistent. For the graphene bio-interface, the nanotexture-induced matching effect [45] obviously enhanced the contact ar-

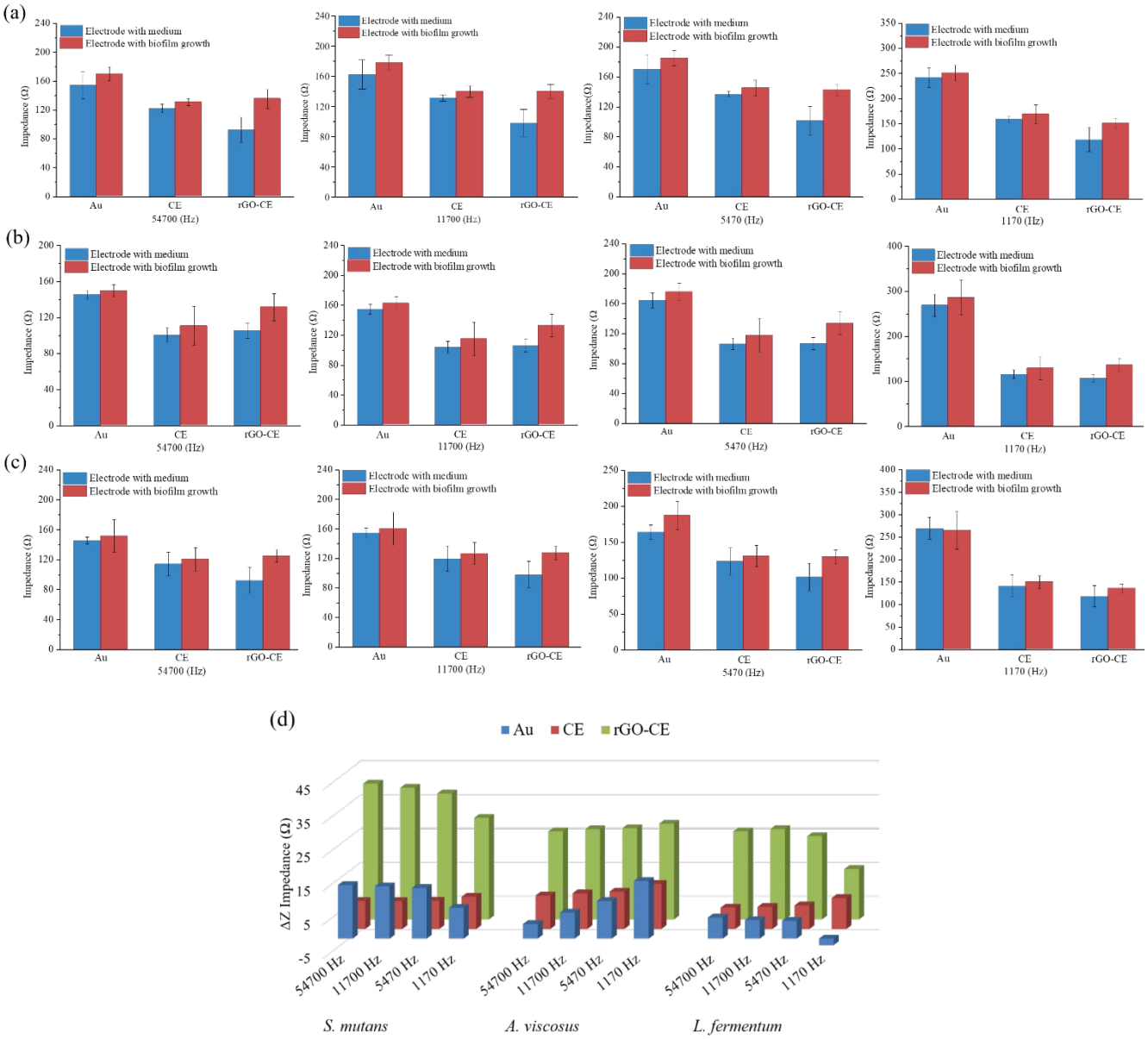

Figure 5. Statistical analysis of the impedance values of *S. mutans* (a), *A. viscosus* (b) and *L. fermentum* (c) attached to the surface of the different electrodes before and after biofilm formation. The data represent the mean of five results ± standard deviation. The *ΔZ* of three kinds of bacteria at different frequencies (d).

ea, which forcefully allowed current penetration into the bacterial biofilms in the attached state. The statistical analysis of the impedance values of the three bacteria at the following four frequencies of 1.17 kHz, 5.47 kHz, 11.7 kHz and 54.7 kHz before and after the attachment of the biofilm on the three electrodes is shown in Figures 5a-c, respectively. The average values are given as the result ± standard deviation. Interestingly, we found that in the same medium environment (electrochemically inert support solution) and at the same frequency, the intrinsic impedance value of the electrode surface of the carbon material and the impedance value after attaching the biofilm were smaller than the impedance value detected on the surface of the Au electrode. This was the same for the entire frequency of 10 Hz~100 kHz, especially below 1 kHz. This could be because that the surface area enhancement and the fluffy wrinkled morphology of carbon material electrodes allow an increase in the charge injection per unit area at the electrode-electrolyte interface, resulting in significant reduction in the electrochemical impedance of the electrodes [46]. Compared with the control group of the biofilm-free state, the three bacteria showed different impedance intensities at the same frequency and the frequency of the maximum impedance increase of the three bacteria were also different. The increment in impedance *ΔZ* of the three bacteria (which was the difference between the impedance of the latter state and that of the former state, for example, $\Delta Z = Z_{biofilm} = Z_{electrode\ with\ biofilm\ growth} - Z_{electrode\ with\ medium}$) obtained at the four frequencies of 1.17 kHz, 5.47 kHz, 11.7 kHz and 54.7 kHz is shown in Figure 5d. The *ΔZ* value of rGO-CE with bacterial growth at the four frequencies was 1.7 to 6.0 times larger than that of the Au electrode and 1.6 to 4.8 times that of the CE. Among them, the impedance signal of *A. viscosus* on rGO-CE was 6.0 times larger than that on the Au electrode at 54.7 kHz, *S. mutans* was 3.3 times larger than that on the Au electrode at 1.17 kHz, and *L. fermentum* was 4.9 times larger than that on the Au electrode at 11.7 kHz (Figure 5d). We ascribed the enhancement of the signal of rGO-CE to a large effective surface area and high electrical conductivity. Additionally, this might be ascribed to the larger number of capture bacteria on rGO-CE than on the Au electrode. Furthermore, stronger changes in impedance measurements indicated that this method might be more suitable for tracking small changes in biofilm growth than Cvio measurements. Unlike the other three frequencies, *L. fermentum* had a negative *ΔZ* (-1.9 Hz) measured with the Au electrode at 1.17 kHz, indicating that the impedance tests before and after biofilm growth based on the Au electrode did not differ at this frequency. Therefore, at least for *L. fermentum*, the impedance detection using the Au electrode at this frequency was not optimal. In addition, we selected two bacteria, *S. mutans* and *A. viscosus*, which produced more biomass, and plotted *ΔZ* at OD590 nm (Figure S6). The results showed that the biomass of the biofilm on rGO-CE of both bacteria had a good correlation with *ΔZ* at the four frequencies. In comparison, the relationship between *ΔZ* and the biomass of *S. mutans* on the Au electrode was irregular and *ΔZ* of *A. viscosus* was negative in the case of a low biomass at 1.17 kHz; thus, for Au electrodes, this frequency was not suitable. This indicates that rGO-CE had a wider detectable frequency range and a superior sensitivity. In short, rGO-CE had inherent advantages over Au electrodes for the detection of three oral bacterial biofilms.

Drug treatment. During mature biofilm formation, 0.075%~0.1% cetylpyridinium chloride (CPC) inhibited dry weight, viability, and acidogenicity [47]. CPC is the main ingredient in common mouthwashes. In the early stage of biofilm maturation, we used EIS to detect the response of Au electrodes, CE and rGO-CE to changes in biofilm impedance after a 0.075% CPC treatment. Three representative frequencies of 5.47 kHz, 11.7 kHz and 54.7 kHz were selected. The impedance value of the drug-treated biofilm was the difference between the drug-treated electrode with an attached biofilm and the drug-treated electrode ($Z_{drug\ treated\ biofilm} = Z_{drug\ treated\ electrode\ with\ biofilm\ attached} - Z_{drug\ treated\ electode}$).

The relative impedance change rate was used to compare the response of the three electrodes to the detection of bacterial biofilm damage, and was calculated as follows: relative impedance change rate = $(Z_{biofilm} - Z_{drug\ treated\ biofilm})/Z_{biofilm} \times 100\%$. After the CPC treatment, the bacterial cell membrane was destroyed, causing damage or death of the bacteria, and the impedance changed accordingly; the results are shown in Table 1. It was clearly indicated that under the same experimental conditions, the biofilm impedance values of the three bacteria treated with 0.075% CPC had different degrees of change. The most obvious of which was the measurement by rGO-CE, where the relative impedance change rate was above 70% at the three detection frequencies. The impedance change rate measured by the Au electrode was obvious at 5.47 kHz, and CE only responded well to the viscous actinomycetes. It was indicated that the CE modified with the *in situ* graphene layer was more sensitive than the Au electrode and CE in estimating the effect of bacterial biofilm destruction owing to a drug. Since the characteristic micro-topology formed by the fluffy graphene layer on rGO-CE surface could produce larger changes in the impedance signal by loading more bacterial biomass, when the bacterial cell became damaged or dead, a loss of the complete cell membrane would also lead to more distinguishable changes in the detected impedance value. It could also be supported by Figure S6, in which a larger *ΔZ* on rGO-CE was found based on the same changing degree of biomass. Table S1 shows the relative impedance change rate produced by the 0.075% CPC itself on different electrode surfaces. It had an impedance signal in the medium with different sucrose concentrations. However, it

was not a threat compared to the relative impedance change rate produced by biofilm disruption. In summary, rGO-CE had a high impedance signal in response to screening for biofilm-damaging drugs.

Circuit model. The Impedance of an electrode is determined primarily by the ion environment both at the electrode/solution interface and in the bulk solution. Under an applied electrical field, the ions undergo field-directed movement and concentration gradient-driven diffusion. The total electrode impedance has two components: the resistance of the electrolyte solution and the impedance at the electrode/solution interface. The presence of the bacteria will affect the local ionic environment at the electrode/solution interface, leading to an increase in the electrode impedance. In the case of non-Faraday impedance detection, i.e. in the absence of a redox probe, the total electrode impedance has three components: the resistance of the electrolyte solution, the impedance of the bacteria, and the impedance at the electrode/solution and electrode/bacteria interfaces. The biological status of the bacteria, including bacterial viability, bacterial number, bacterial morphology, and degrees of adhesion, will affect the measurement of electrode impedance [48].

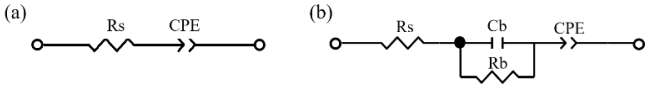

Figure 6. Equivalent circuit model for the interaction on the electrode without (a) a biofilm and with (b) a biofilm.

An electrical equivalent circuit model of the biofilms attached to the electrode interface is provided to better understand the biofilm-electrode interaction. The electric behaviour of the electrode in a BHI medium with and without biofilm can be represented by the equivalent circuit shown in Figure 6.

In our circuit, the double-layer capacitor was connected in series to R_s, which was determined by the ion concentration in the solution between the working electrode and the reference electrode. After the biofilm was formed, the capacitance of the biofilm C_b was introduced in parallel with the biofilm resistance R_b [49, 50]. However, due to the unevenness of the electrode surface that we could clearly see from Figure 2, the double-layer capacitance at the electrode interface deviated from the nature of an ideal capacitance, so a constant phase element was introduced to represent the capacitance impedance of the electrode interface. The impedance of the constant phase element, which represents the interfacial capacitance impedance, was defined as $Z_{CPE} = \frac{1}{Q}(j\omega)^{-n}$, where ω is the angular frequency, Q is the magnitude of Z_{CPE}, and n is a constant ($0 \le n \le 1$) representing the inhomogeneity in the surface [51]. Thus, the entire impedance of the biofilm-electrode interface could be defined as (Eq. (2)):

$$Z_{with\ biofilm} = R_s + \frac{R_b}{1 + R_b j\omega C_b} + Z_{CPE} \quad (2)$$

Table 1. Relative impedance change rate of bacterial biofilm after the CPC treatment at 54.7 kHz, 11.7 kHz and 5.47 kHz. (n=5).

Frequency	*S. mutans*			*A. viscosus*			*L. fermentum*		
	Au	CE	rGO-CE	Au	CE	rGO-CE	Au	CE	rGO-CE
54700 Hz	24.8%	33.2%	84.3%	29.5%	61.3%	75.1%	3.8%	30.3%	85.4%
11700 Hz	31.3%	22.4%	80.2%	44.3%	65.0%	72.8%	16.4%	33.2%	76.7%
5470 Hz	48.1%	23.6%	78.7%	75.8%	66.7%	73.0%	64.9%	37.0%	74.3%

Based on our circuit model, we fitted the parameters of the three bacteria on the three electrodes in Figure 6 (which had a χ^{-2} value of 10^{-3}). The data are summarized in Tables S2-S4. It should be noted here that the fitted R_s was not necessarily a solution resistance. It included all possible ohmic resistances in the electrode system, and the ohmic resistances of the electrodes themselves due to differences in conductivity were one of them [50]. Therefore, as seen in the three tables below, the initial R_s measured by the three electrodes of each bacteria in their own broth varied. The R_s values of all three electrodes increased after the biofilm was formed on them. rGO-CE increased by 36.5 Ω compared with13.4 Ω with the Au electrodes and 4.7 Ω with CE, as shown in Tables S2-S4 also showed the same trend. After the growth of the biofilm, even the CPE changed, but the change trend of the CPE with the three kinds of bacteria in the low frequency region was different, such as the increase of CPE with *S. mutans* and *L. fermentum*, and the decrease of CPE with *A. viscosus*. Although R_b and C_b were generated in the formation of biofilms, the total impedance changes of the two in parallel was not as obvious as in the high frequency region. In our test range, the frequency region represented by R_s was between 10 and 100 kHz for the Au electrode, and between 1 and 100 kHz for the carbon material electrode. This could be seen from the phase angles being close to 0 deg in the phase diagrams of Figures 4b-f, which was also exactly the area where we directly selected the characteristic frequency by relying on the magnitude of the change. Therefore, we concluded that regardless of which electrode was used, the increase of the impedance signal after biofilm formation was mainly caused by the increase in the medium resistance R_s.

CONCLUSIONS

CE modified with an electrochemically *in situ* generated graphene layer has obvious advantages over Au electrodes with the use of EIS to detect bacterial biofilms. When bacterial biofilms grow on the surface, the ΔZ value of rGO-CE is 1.7~6.0 times that of the Au electrode at 5.47 kHz, 11.7 kHz and 54.7 kHz. In particular, the impedance signal of *A. viscosus* on rGO-CE is 6.0 times larger than that of the Au electrode at 54.7 kHz. Furthermore, when using the rGO-CE interface for drug test, the relative impedance change rates of the three bacteria after a 0.075% CPC treatment were more than 70% at three detection frequencies. Furthermore, greater loading of biomass on the rough surface of rGO-CE enables the destruction of the biofilm by drug to be detectable, which is undetectable by the Au electrode. The results confirmed our hypothesis that compared to the classic Au interface, *in situ* generated graphene as an interface material for impedance detection can significantly enhance the impedance sensing sensitivity to bacterial biofilm growth and decay by increasing bacterial capture efficiency. It is promising to develop a graphene-based impedance biosensor platform for biofilm study and anti-biofilm drug screening.

ASSOCIATED CONTENT

Supporting Information. All materials, reagents, instruments, experimental methods used in this study and more information are described in detail in the Supporting Information.

AUTHOR INFORMATION

Corresponding Authors

* Email: zhangxe@ibp.ac.cn

* Email: yuanqp@mail.buct.edu.cn.

Author Contributions

The manuscript was written through contributions of all authors.

Notes

The authors declare no competing financial interest.

ACKNOWLEDGMENT

This work was supported by the National Natural Science Foundation of China (Grant No. 2189074), the Strategic Priority Research Program of the Chinese Academy of Sciences, China (Grant No. XDB29050100). We thank Yu Hou, Tingting Wang, Xia Li and Nan Shao for helpful discussions. Technical service from Core Facility and Technical Support, Institute of Microbiology and Institute of process engineering, Chinese Academy of Sciences are also acknowledged.

REFERENCES

1. Joana, A.; Nuno, F.A.; Romain, B.; Nuno, C.; Tom, C.; Ana, R.C.; Mickaël, D.; Giovanni, D.B.; Michel, H.; Zoran, J.; Miroslava, K.; Susanne, K.; Anália, L.; Filipe, M.; Rikke, L.M.; George, N.; Manuel, S.; Odile, T.; Claus, S. Critical review on biofilm methods. Crit Rev Microbiol. 2017, 43, 313-351.
2. Hilary, M.L.S.; J. William, C. Microbial Biofilms, Cambridge University Press: Cambridge, 2003.
3. Marsh P.D. Dental plaque: biological significance of a biofilm and community life-style. J Clin Periodontol. 2005, 32, 7-15.
4. Pohlscheidt, M.; Charaniya, S.; Bork, C.; Jenzsch, M.; Noetzel, T.L.; Luebbert, A. Bioprocess and fermentation monitoring, Wiley: Hoboken, 2013.
5. Giaever, I.; Keese, C.R. Monitoring fibroblast behavior in tissue culture with an applied electric field. Proc. Natl. Acad. Sci. U.S.A. 1984a, 3761-3764.
6. Giaever, I.; Keese, C.R. Micromotion of mammalian cells measured electrically. Proc. Natl. Acad. Sci. U.S.A. 1991b, 88, 7896-7900.
7. Dheilly, A.; Linossier, I.; Darchen, A.; Hadjiev, D.; Corbel, C.; Alonso, V. Monitoring of microbial adhesion and biofilm growth using electrochemical impedancemetry. Appl Microbiol Biotechnol. 2008, 79, 157-164.
8. Sheng, X.X.; Ting, Y.P.; Pehkonen, S.O. The influence of sulphate-reducing bacteria biofilm on the corrosion of stainless steel AISI 316. Corrosion Science. 2007, 49, 2159-2176.
9. Souza, J.G.S.; Cordeiro, J.M.; Lima, C.V.; Barão, V.A.R. Citric acid reduces oral biofilm and influences the electrochemical behavior of titanium: An in situ and in vitro study. J Periodontol. 2019, 90, 149-158.
10. Bayoudh, S.; Othmane, A.; Ponsonnet, L.; Ben Ouada, H. Electrical detection and characterization of bacterial adhesion using electrochemical impedance spectroscopy-based flow chamber. Colloids Surf. A: Physicochem. Eng. Asp. 2008, 318, 291-300.
11. Ben-Yoav, H., Freeman, A., Sternheim, M., Shacham-Diamand, Y. An electrochemical impedance model for integrated bacterial biofilms. Electrochim. Acta. 2011, 56(23), 7780-7786.
12. Muñoz-Berbel, X.; García-Aljaro, C.; Muñoz, F.J. Impedimetric approach for monitoring the formation of biofilms on metallic surfaces and the subsequent application to the detection of bacteriophages. Electrochim. Acta. 2008, 53(19), 5739-5744.
13. Garcia, S.N.; Gutierrez, L.; McNulty, A. Real-time cellular analysis as a novel approach for in vitro cytotoxicity testing of medical device extracts. J Biomed Mater Res Part A. 2013, 101A, 2097-2106.
14. Jacobo, P.; Sheila, B., Sergio, A. Label-free interdigitated microelectrode based biosensors for bacterial biofilm growth monitoring using Petri dishes. J Microbiol Meth. 2014, 100,77-83.
15. Gutiérrez, D.; Hidalgo-Cantabrana, C.; Rodríguez, A.; García, P.; Ruas-Madiedo, P. Monitoringin Real Time the formation and removal of biofilms from clinical related pathogens using an impedance-based technology. PLoS One. 2016, 11, e0163966.
16. Anh-Nguyen, T.; Tiberius, B.; Pliquett, U.; Urban, G.A. An impedance biosensor for monitoring cancer cell attachment, spreading and drug-induced apoptosis. Sensor Actuat A-Phys. 2016, 241, 231-237.
17. van Duuren, J.B.J.H.; Müsken, M.; Karge, B.; Tomasch, J.; Wittmann, C.; Häussler, S.; Brönstrup, M. Use of single-frequency impedance spectroscopy to characterize the growth dynamics of biofilm formation in Pseudomonas aeruginosa. Sci Rep. 2017, 7, 5223.
18. Xu,Y.K.; Dhaouadi, Y.; Stoodley, P.; Dacheng, Ren. Sensing the unreachable: challenges and opportunities in biofilm detection. Curr Opin Biotech. 2020, 64:79-84.
19. Pandele, A.M.; Ionita, M.; Crica, L.; Dinescu, S.; Costache, M.; Iovu, H. Synthesis, characterization, and in vitro studies of graphene oxide/chitosan–polyvinyl alcohol films. Carbohyd Polym. 2014, 102, 813-820.
20. Ioniţă, M.; Vlasceanu, G.M.; Watzlawek, A.A.; Voicu, S.I.; Burns, J.S.; Iovu, H. Graphene and functionalized graphene:

Extraordinary prospects for nanobiocomposite materials. Compos Part B. 2017, 121, 34-57.
21. Li, M.; Xiong, P.; Yan, F.; Li, S.J.; Ren, C.H.; Yin, Z.C.; Li, A.; Li, H.F.; Ji, X.M.; Zheng, YF.; Cheng, Y. An overview of graphene-based hydroxyapatite composites for orthopedic applications. Bioactive Materials. 2018, 3, 1-18.
22. Wang, X.H.; Liu, A.P.; Xing, Y.; Duan, H.W.; Xu, W.Z.; Zhou, Q.; Wu, H.P.; Chen, C.; Chen, B.Y. Three-dimensional graphene biointerface with extremely high sensitivity to single cancer cell monitoring. Biosens. Bioelectron. 2018,105, 22-28.
23. Li, Y.W., Zhou. J., Song, J., Liang, X.S., Zhang, Z.P., Men, D., Wang, D.B., Zhang, X.E., Chemical nature of electrochemical activation of carbon electrodes. 2019. Biosens. Bioelectron. 149, 111874.
24. Ranganathan, V.; Akhila, C.H. Streptococcus mutans: has it become prime perpetrator for oral manifestations? J. Microbiol. Exp. 2019, 7, 207-213.
25. Salas-Jara, M.J.; Ilabaca, A.; Vega, M.; García, A. Biofilm Forming Lactobacillus: New Challenges for the Development of Probiotics. Microorganisms. 2016, 4(3), 35.
26. Balto, H.A.; Shakoor, Z.A.; Kanfar, M.A. Combined effect of a mixture of tetracycline, acid, and detergent, and nisin against Enterococcus faecalis and Actinomyces viscosus biofilms. Saudi Med J. 2015, 36(2), 211-215.
27. Ferrer, M.D.; Rodriguez, J.C.; Alvarez, L.; Artacho, A.; Royo, G.; Mira, A. Effect of antibiotics on biofilm inhibition and induction measured by real-time cell analysis. J Appl Microbiol. 2017, 122, 40-650.
28. Cheng, Q.; Tang, J.; Ma, J.; Zhang, H.; Shinya, N.; Qin, L.C. Graphene and nanostructured MnO2 composite electrodes for supercapacitors. J. Phys. Chem. 2011, 115, 23584-23590.
29. Palanisamy, S.; Karuppiah, C.; Chen, S.M.; Periakaruppan, P. Highly sensitive and selective amperometric nitrite sensor based on electrochemically activated graphite modified screen printed carbon electrode. J Electroanal Chem. 2014, 727, 34-38.
30. Zhang, H., Li, S., Zhang, F.H., Wang M.X., Lin, X.C., Li, H.X., Simultaneous detection of hydroquinone and catechol on electrochemical-activated glassy carbon electrode by simple anodic and cathodic polarization. J Solid State Electrochem. 2016, 21, 1-11.
31. Liu, S.B.; Zeng, T.H.; Hofmann, M.; Burcombe, E.; Wei, J.; Jiang, R.R.; Kong, J.; Chen, Y. Antibacterial activity of graphite, graphite oxide, graphene oxide, and reduced graphene oxide: Membrane and oxidative stress. Acs Nano. 2011, 5, 6971-6980.
32. Wong, C.P.P.; Lai, C.W.; Lee, K.M.; Hamid, B.S.A. Materials. Advanced chemical reduction of reduced graphene oxide and its photocatalytic activity in degrading reactive black 5. 2015, 8, 7118-7128.
33. Sur, U.K.; Saha, A.; Datta, A.; Ankamwar, B.; Surti, F.; Roy, S.D.; Roy, D. Synthesis and characterization of stable aqueous dispersions of graphene. Bull Mater Sci. 2016, 39, 159.
34. Alam, S.N.; Sharma, N.; Kumar, L. Synthesis of graphene oxide (GO) by modified Hummers method and its thermal reduction to obtain reduced graphene oxide (rGO). Graphene, 2017, 6, 1-18.
35. Bowling, R.; Packard, R.T.; McCreery, R.L. Activation of highly ordered pyrolytic graphite for heterogeneous electron transfer: Relationship between electrochemical performance and carbon microstructure. Langmuir. 1989, 5, 683-688.
36. Lim, C.X.; Hoh, H.Y.; Ang, P.K.; Loh, K.P. Direct voltammetric detection of DNA and pH sensing on epitaxial graphene: An insight into the role of oxygenated defects. Anal. Chem. 2010, 82, 7387-7393.
37. Bard, A.J.; Faulker, L.R.L.R. Electrochemical Methods: Fundamentals and Applications, John Wiley: New York, 2000.
38. Gabriela, P.M. Confocal scanning laser microscopy in the study of biofilm formation in tissues of the upper airway in otolaryngologic diseases. Microscopy: Science, Technology, Applications and Education. 2011, 590-596.
39. Bai, L.; Chen, Y.; Bai, Y.; Zhou, J.; Huang, A. Fullerenedoped polyaniline as new redox nanoprobe and catalyst in electrochemical aptasensor for ultrasensitive detection of Mycobacterium tuberculosis MPT64antigen in human serum. 2017, Biomaterials, 133, 11-19.
40. Hu, K.C.; Lan, D.X.; Li, X.M.; Zhang, S.S. Electrochemical DNA biosensor based on nanoporous gold electrode and multifunctional encoded DNA-Au bio bar codes. Enzyme Microb. Anal. Chem. 2008, 80, 9124-9130.
41. Tomás, I.; García-Caballero, L.; Cousido, M.; Limeres, J.; Álvarez, M.; Diz, P. In vivo oral biofilm analysis by confocal laser scanning microscopy: methodological approaches. Oral Dis. 2009, 15, 428-433.
42. O'Toole, G.A.; Kolter, R. Initiation of biofilm formation in Pseudomonas fluorescens WCS365 proceeds via multiple, convergent signaling pathways: a genetic analysis. Mol. Microbiol. 1998, 28, 449-461.
43. Harris, C.M.; Todd, R.W.; Bungard, S.J.; Lovitt, R.W.; Morris, J.G.; Kell, D.B. The dielectric permittivity of microbial suspensions at radio frequencies: a novel method for the real-time estrmation of microbial biomass. Enzyme microb Tech. 1987, 9, 181-186.
44. Carvell, J.P.; Dowd, J.E. On-line measurements and control of viable cell density in cell culture manufacturing processes using radio-frequency impedance. Cytotechnology. 2006, 50, 35-48.
45. Li, Y., Lu, Q., Liu, H., Wang, J., Zhang, P., Liang, H., Jiang, L., Wang, S., Antibody modified reduced graphene oxide film with extreme sensitivity to circulating tumor cells. Adv. Mater. 2015, 27, 6848-6854.
46. Gaio, N., Silvestri, C., van Meer, B., Vollebregt, S., Mummery, C.L., Dekker, R. Fabrication and characterization of an upside-down Carbon Nanotube (CNT) Microelectrode array (MEA). IEEE Sens J. 2016, 16, 8685-8691.
47. Pandit, S.; Cai, J.N.; Jung, J.E.; Lee, Y.S.; Jeon, J.G. Effect of brief cetylpyridinium chloride treatments during early and mature cariogenic biofilm formation. Oral Dis. 2015, 21, 565-571.
48. Solly, K.; Wang, X.B.; Xu, X.; Strulovici, B.; Zhang, W. Application of Real-Time Cell Electronic Sensing (RT-CES) Technology to Cell-Based Assays. Assay Drug Dev Technol. 2004, 2, 363-372.
49. González, J.E.G.; Santana, F.J.H.; Mirza-Rosca, J.C. Effect of bacterial biofilm on 205 SS corrosion in natural seawater by EIS. Corros Sci. 1998, 40, 2141-2154.
50. Sheng, X.X.; Ting, Y.P.; Pehkonen, S.O. The influence of sulphate-reducing bacteria biofilm on the corrosion of stainless steel AISI 316. Corros Sci. 2007, 49, 2159-2176.
51. Jia, Z.; Dai C.S.; Chen, L. Electrochemical measurement method, Chemical Industry Press: Beijing, 2006.

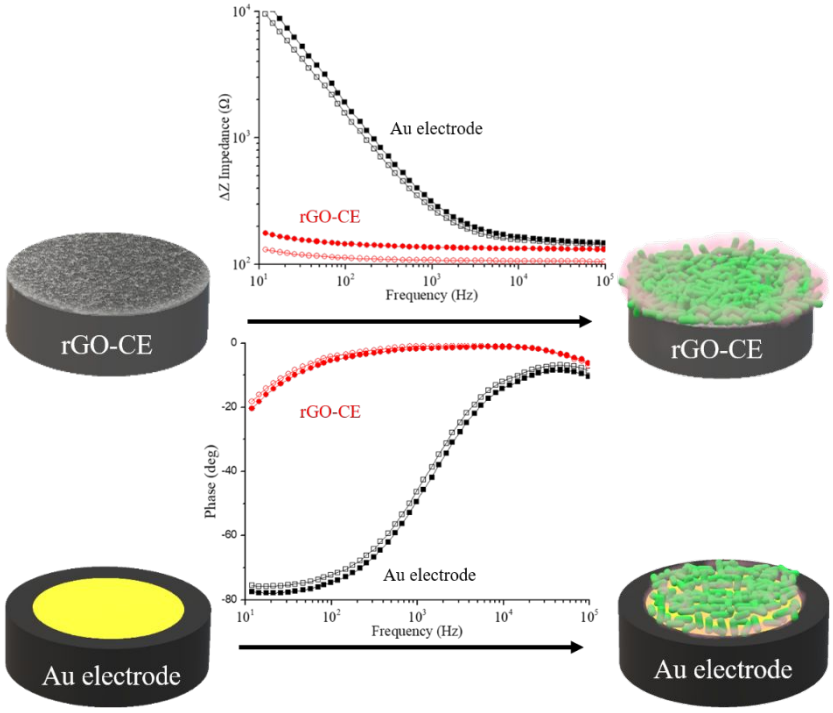
ΔZ Impedance (Ω)
Au electrode
rGO-CE
Frequency (Hz)
rGO-CE
rGO-CE
Phase (deg)
rGO-CE
Au electrode
Frequency (Hz)
Au electrode
Au electrode

for TOC only